HYDROLOGICAL PROCESSES
Hydrol. Process. (2011)
Published online in Wiley Online Library
(wileyonlinelibrary.com) DOI: 10.1002/hyp.8158

Modelling catchment-scale shallow landslide occurrence and sediment yield as a function of rainfall return period

C. I. Bovolo* and J. C. Bathurst

Water Resource Systems Research Laboratory, School of Civil Engineering and Geosciences, Newcastle University, Newcastle upon Tyne, NE1 7RU, UK

Abstract:

A model-based method is proposed for improving upon existing threshold relationships which define the rainfall conditions for triggering shallow landslides but do not allow the magnitude of landsliding (i.e. the number of landslides) to be determined. The SHETRAN catchment-scale shallow landslide model is used to quantify the magnitude of landsliding as a function of rainfall return period, for focus sites of 180 and 45 km^2 in the Italian Southern Alps and the central Spanish Pyrenees. Rainfall events with intensities of different return period are generated for a range of durations (1-day to 5-day) and applied to the model to give the number of landslides triggered and the resulting sediment yield for each event. For a given event duration, simulated numbers of landslides become progressively less sensitive to return period as return period increases. Similarly, for an event of given return period, landslide magnitude becomes less sensitive to event duration as duration increases. The temporal distribution of rainfall within an event is shown to have a significant impact on the number of landslides and the timing of their occurrence. The contribution of shallow landsliding to catchment sediment yield is similarly quantified as a function of the rainfall characteristics. Rainfall intensity–duration curves are presented which define different levels of landsliding magnitude and which advance our predictive capability beyond, but are generally consistent with, published threshold curves. The magnitude curves are relevant to the development of guidelines for landslide hazard assessment and forecasting. Copyright © 2011 John Wiley & Sons, Ltd.

KEY WORDS catchment model; debris flow; landslide magnitude; rainfall intensity-duration; rainfall return period; sediment yield; shallow landslide; SHETRAN

Received 7 June 2010; Accepted 18 April 2011

INTRODUCTION

An important component of landslide hazard assessment is predicting landslide occurrence and impact. Much past work has been devoted to quantification of the conditions under which shallow landslides may be triggered (e.g. as a function of rainfall intensity and duration, Caine (1980)) and to recording the nature of specific landslide events (e.g. Chen *et al*., 2005). Only relatively recently has research started to quantify, not just the triggering conditions, but the extent of shallow landslide occurrence (i.e. spatial distribution and numbers of slides) as a function of rainfall return period, raising the possibility of issuing warnings of landslide severity on the basis of weather forecasts (e.g. Crozier and Glade, 1999; Dhakal and Sidle, 2004; Falorni *et al*., 2007; Schmidt *et al*., 2008). Further, very little of this work has considered the offsite impact of landslide events (such as downstream sediment yield), and much of the relevant modelling work has been limited to areas of a few square kilometres or less. There are considerable practical difficulties in obtaining data on landslide occurrence, sediment yield and rainfall frequency for events of different sizes at large catchment scales. As a result, for the time being, progress in the wider topic is likely to depend on modelling studies rather than data-based research. The aim of this paper is therefore to propose a model-based methodology for quantifying the magnitude of shallow landslide events and their sediment yield as a function of rainfall return period, for rainfalls of different combinations of intensity and duration. Using a shallow landslide sediment yield model integrated with a distributed, physically based hydrological, erosion and sediment yield modelling system, simulations are carried out for focus catchments of area 180 and 45 km^2 in the Italian Southern Alps and the central Spanish Pyrenees respectively. Rainfall events with intensities of different return period are generated for a range of durations (1-day to 5-day) and applied to the model to give the number of landslides triggered and the resulting sediment yield for each event. The results are then used to develop a method for presenting landslide magnitudes on rainfall intensity/duration graphs in a way which complements but advances beyond the existing threshold curves for landslide occurrence. The work formed a component of the European Commission-funded LESSLOSS project on Risk Mitigation for Earthquakes and Landslides (http://www.lessloss.org/) and builds on earlier work in the European Community-funded DAMOCLES project on debris flow hazard assessment (Bathurst *et al*., 2003; http://damocles.irpi.cnr.it/).

* Correspondence to: C. I. Bovolo, Water Resource Systems Research Laboratory, School of Civil Engineering and Geosciences, Newcastle University, Newcastle upon Tyne, NE1 7RU, UK.
E-mail: isabella.bovolo@ncl.ac.uk

Copyright © 2011 John Wiley & Sons, Ltd.

LANDSLIDE INCIDENCE AND RAINFALL CHARACTERISTICS

There has been a recent trend in landslide research towards quantifying the temporal frequency and magnitude of landslides and debris flows (e.g. Crozier and Glade, 1999; D'Agostino and Marchi, 2001; Reid and Page, 2002; Jakob *et al*., 2005). A variety of approaches have been followed, usually relating landslide magnitude to storm rainfall. However, while the number of landslides generally increases with rainfall magnitude, rainfall frequency does not translate exactly into landslide frequency. Shallow landslides are generally considered to be caused by high porewater pressures in the soil, but the extent to which porewater conditions are related to rainfall depends on soil properties, antecedent moisture conditions and other variables which exhibit considerable spatial and temporal variability (Reichenbach *et al*., 1998). Account must therefore be taken of the intervening behaviour and properties of the hillslope system (Crozier and Glade, 1999). This can be achieved by a variety of modelling approaches.

Crozier and Glade (1999) note that the frequency–magnitude characteristics of landslide activity can be investigated both empirically and deterministically. The empirical approach depends on the availability of sufficient data and typically involves the quantification of a range of rainfall thresholds for triggering shallow landslides. At the simplest level such thresholds separate the occurrence and non-occurrence of shallow landslides. A well-known example is Caine's (1980) intensity-duration threshold formula, based on data from 73 studies of shallow landslides around the world and applicable for rainfall durations of between 10 min and 10 days:

$$I = 14{\cdot}82\ D^{-0{\cdot}39} \tag{1}$$

where I is the mean storm rainfall intensity (mm h^{-1}) and D is the storm duration (h). More recently Crosta and Frattini (2001) have presented a threshold curve of the form

$$I = a((b/D) + c) \tag{2}$$

where a, b and c are coefficients. For a curve which encompasses almost all the data available to those authors on a global scale, $a = 8$, $b = 0{\cdot}9$ and $c = 0{\cdot}06$. For a local curve relevant to the Italian Southern Alps, $a = 12$, $b = 1$ and $c = 0{\cdot}07$. Most comprehensively, Guzzetti *et al*. (2008) analyse a large data base to present new global threshold curves varying with analytical method and range of rainfall duration. Brunetti *et al*. (2010) subsequently use the data relevant to Italy to define national and regional threshold curves. Any combination of storm intensity and duration such that intensity exceeds the threshold value given by such curves is likely to cause widespread shallow landslide activity. The approach can also be refined to account for the moderating influence of antecedent soil moisture (Crozier and Eyles, 1980; Sidle and Ochiai, 2006, 147–149). Sidle *et al*. (1985, 90–93) indicate that such relationships can be of use in identifying return periods for various combinations of rainfall intensity and duration that will probably induce landsliding. However, the approach refers only to whether or not landslides will occur and not to the magnitude or severity of an event, e.g. the number of landslides which may occur.

The deterministic approach to quantifying frequency–magnitude relationships involves the use of physically based, spatially distributed landslide models. These integrate hydrological models with geotechnical slope stability models and enable slope stability to be investigated as a function of rainfall. Such models have been developed both for detailed slope investigations (e.g. Wilkinson *et al*., 2002) and for more general catchment-scale studies (e.g. Montgomery and Dietrich, 1994; Wu and Sidle, 1995; Burton and Bathurst, 1998; Gorsevski *et al*., 2006). In principle, they can be used to determine not only rainfall thresholds for landslide occurrence but also the magnitude or extent of the landsliding. Application of different rainfalls then allows the simulated landslide magnitude to be related to rainfall frequency. Difficulties with the approach arise from the characteristic uncertainties of the modelling process: these include the extent to which the relevant physical processes are represented, the provision of the necessary topographic, soil and vegetation data, the uncertainty inherent in parameterizing models with large numbers of parameters and the spatial resolution of the model. The literature contains only a few examples of this approach (e.g. Iida, 2004; Dhakal and Sidle, 2004; Frattini *et al*., 2009). Generally, they are concerned only with landslide and debris flow occurrence on hillslopes and in headwater streams and do not consider the off-site impacts of landsliding, such as sediment delivery into the downstream river-channel network.

This paper follows the deterministic approach to investigate the relationship between rainfall frequency and the magnitude of shallow landslide events, including event impact. The application highlights both the capabilities and the difficulties of the approach.

SHETRAN SHALLOW LANDSLIDE MODEL

Model background

The study uses the SHETRAN shallow landslide and sediment yield model; this is fully described by Burton and Bathurst (1998), so only a summary is given here. The model is a component of the SHETRAN physically based, spatially distributed, catchment modelling system (described by Ewen *et al*., 2000), that provides the hydrological and sediment transport framework for simulating rain- and snowmelt-triggered landsliding and its sediment yield. (Details are available at http://research.ncl.ac.uk/shetran/) The hydrological model accounts in a fully integrated way for vegetation interception and transpiration, snowmelt, overland flow, subsurface unsaturated and saturated flow and river/aquifer interaction. The version of SHETRAN used in this application (v3.4) simulates an unconfined aquifer

Copyright © 2011 John Wiley & Sons, Ltd.

composed of a one-dimensional (vertical flow) unsaturated zone overlying a two-dimensional (horizontal flow) saturated zone, with a dynamic phreatic surface as the interface between the two. Complementing the hydrological model is a conventional sediment transport model in which sediment yield is determined as a function of soil erosion by raindrop impact and overland flow and transport by overland and channel flow. The model requires spatially variable data for topography and for vegetation, soil, sediment and geotechnical properties, and spatially variable time-series of precipitation and evaporation to drive the model.

In the landslide model, the occurrence of shallow landslides is determined as a function of the time- and space-varying soil saturation conditions simulated by the hydrology model, using standard, geotechnical, infinite-slope, factor-of-safety analysis. This includes allowance for the effect of vegetation root cohesion. However, in line with observation and theory (e.g. Sidle *et al*., 1985) shallow landslides are not simulated for slopes of less than 25°. For each landslide, the volume of eroded material is determined from the soil depth and the area of the landslide. Eroded material is routed down the hillslope as an unconfined debris flow if the vegetation is forest or if the landslide occurs in a gully. However, if the landslide occurs on a planar grass-covered slope, there is no onward transport and the landslide is assumed to be a slump. This rule-based approach was based on experience in New Zealand (personal communication to Bathurst by New Zealand researchers, 1990) but it is recognized that it is not likely to be fully accurate in all cases. The role of debris flows in transporting landslide material to the channel network is highlighted by Johnson *et al*. (2000) and Acharya *et al*. (2009) among others. The model also has an option to allow the debris flow to collect additional sediment by scouring along its track (although this was not applied in the cases described here). Deposition by the debris flow starts to occur once the hillslope gradient falls below a certain critical value (the default being 10°) and takes place over the run-out distance, which is calculated as a percentage of the difference in elevation between the landslide location and the critical slope (the default percentage being 40%). At slopes less than 4° the debris flow halts unconditionally and deposits any remaining material. The proportion of the material reaching the channel network is then calculated and fed to the SHETRAN sediment transport model for routing as conventional channel sediment load to the catchment outlet. Material deposited along the track of the debris flow may subsequently be washed into the channel by overland flow and will contribute to the sediment yield totals.

It is emphasized that the model simulates shallow landslides and unconfined debris flows that develop only on hillslopes outside the channel network. Confined debris flows along the channel network, including related channel scour, are not simulated.

Within the main SHETRAN model, the spatial distribution of catchment properties, rainfall input and hydrological response is achieved in the horizontal direction through the representation of the catchment and its channel system by an orthogonal grid network and in the vertical direction by a column of horizontal layers at each grid square. Grid resolution is typically large, however, (as much as 1 or 2 km) compared with the length dimensions of shallow landslides (typically around 10–100 m). The central feature of the landslide model, therefore, is the use of derived relationships (based on a topographic index) which link the larger SHETRAN grid resolution at which the basin hydrology and sediment yield are modelled, to a sub-grid resolution at which landslide occurrence and erosion is modelled. That is, using the topographic index, the SHETRAN grid saturated zone thickness is distributed spatially at the sub-grid resolution. If the factor-of-safety analysis indicates slope failure at a sub-grid element, that element counts as one landslide; also the element can fail only once during the simulation, i.e. only one landslide can be registered at the element. Through this dual resolution design, the model is able to represent landsliding at a physically realistic scale while remaining applicable at catchment scales (up to 500 km^2) likely to be of interest, for example feeding a reservoir. The sub-grid discretization, landslide susceptibility and potential landslide impact (e.g. sediment delivered to the stream system) are determined in advance using a Geographical Information System and this information is stored in a 'look-up' table. During the time-varying simulation, SHETRAN provides information on the temporal variation in soil moisture content as input to the landslide model. As landslides occur, their pre-determined sediment impacts are passed to the SHETRAN sediment transport component from the look-up table and the sediment delivered to channels is routed along the channel system as conventional sediment load to the basin outlet.

Applications of the landslide model are described by Bathurst *et al*. (2005, 2006, 2007). Some recent examples of applications of the SHETRAN hydrological and sediment transport model are presented by Lukey *et al*. (2000), Bathurst *et al*. (2002, 2004) and Adams *et al*. (2005).

FOCUS CATCHMENTS

The focus sites are the 180 km^2 Valsassina-Esino catchment in the Italian Southern Alps and the 45 km^2 Ijuez catchment in the central Spanish Pyrenees (Figure 1). Both sites were originally selected for SHETRAN applications in the DAMOCLES project (Bathurst *et al*., 2003). The Valsassina-Esino catchment was also selected for analysis by Frattini *et al*. (2009). The reader should note that the SHETRAN models used here were originally created, calibrated and applied in the DAMOCLES project (Bathurst *et al*., 2005 and 2007) and that the work reported here builds upon those previous models and results. As full details of the sites, the data collection

Copyright © 2011 John Wiley & Sons, Ltd.

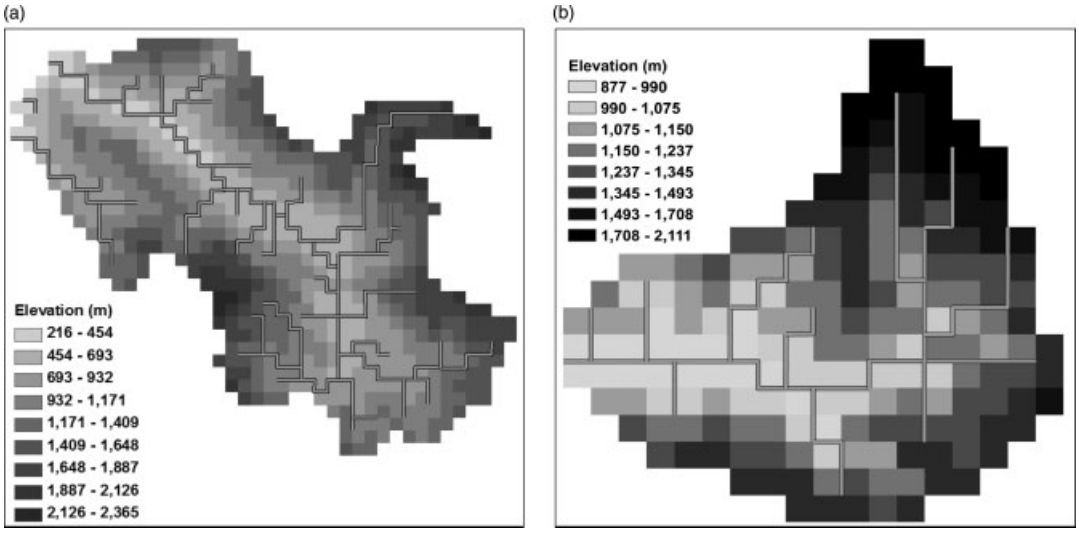

Figure 1. SHETRAN grid network, channel system (thick lines) and elevation distribution for the Valsassina (a) and Ijuez (b) catchments. The grid squares have dimensions 500 m × 500 m

to support the applications and the model parameters are given by Bathurst *et al*. (2005, 2007) respectively, they are only summarized here.

The Valsassina catchment

Valsassina is a wide glaciated valley with a U-shaped profile and hanging valleys. The main river (the Pioverna) discharges into Lake Como (also known as Lake Lario) near Bellano, where the catchment area is 160 km^2. The total area modelled with SHETRAN was actually 180 km^2, incorporating the neighbouring 20 km^2 Esino catchment which also discharges directly into Lake Como. Elevation ranges from 197 m at Lake Como to 2554 m. The valley corresponds to a fault line that separates two geological systems which are of a varied nature but with notable occurrences of Permian and Triassic sedimentary rocks. There are four main land covers: meadows and grass in the valley bottom; forest on the valley sides up to around 1000 m; grass and meadows at elevations up to about 1500 m; and bare rock at higher elevations. From a field survey, three main soil textures (sandy, silt loam; sandy loam; and silt clay) were identified. Mean annual rainfall is around 1240 mm at Bellano and around 1540 mm at Barzio, towards the head of Valsassina.

The original model parameterization and calibration are described by Bathurst *et al*. (2005). Using a 20-m resolution digital elevation model (DEM), the SHETRAN grid was discretized with a 500 m resolution and the landslide-model sub-grid resolution was set at 20 m. Spatial variability was modelled in overland flow resistance, evapotranspiration and root cohesion as a function of vegetation (three types) and in soil hydraulic and geotechnical properties as a function of soil texture (three textures). Soil depth varied according to soil texture and geology (1·5–3 m). A nominal uniform soil depth of

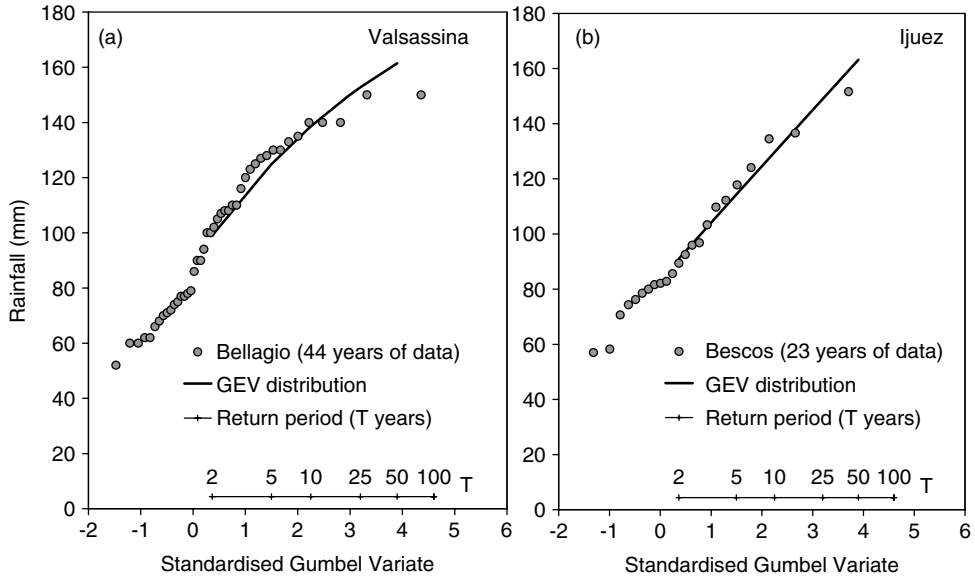

Figure 2. Gumbel plots for annual maximum rainfall of 1-day duration for the Valsassina catchment and 4-day duration for the Ijuez catchment

Copyright © 2011 John Wiley & Sons, Ltd.

0·2 m was used to allow for hydrological response in local occurrences of soil, regolith and coarse debris in areas classified as bare rock. However, shallow landslides were not allowed to occur in these areas. For a simulation period of 6 years and using data from six rain gauges to represent spatial variability in input, the hydrological component was calibrated against regionally derived discharge data (including normalized flow duration curves). In calibrating the hydrology model, adjustments were made to several of the parameters to which the results are most sensitive: the overland flow resistance coefficient, the ratio of actual to potential evapotranspiration at soil field capacity, the soil moisture content/tension property curve and the soil saturated zone hydraulic conductivity (see Bathurst *et al*. (2005) for details). The landslide component was tested against an inventory map of landslide occurrence in Valsassina (compiled for a 50-year period from the 1950s to the present day), showing good spatial representation of the observed pattern. The sediment transport and yield component was calibrated against regional data.

The Ijuez catchment

The Ijuez is a tributary of the Aragón river, 10 km from the city of Jaca. Elevations in the catchment range from 838 to 2173 m, the main lithology is calcareous flysch and the natural vegetation is mainly pines, shrubs and, in the highest parts, meadows. Part of the catchment was reforested in 1955–1956. From a field survey, two main soil textures (silty clay and silty clay loam) were identified. Mean annual rainfall at Jaca is 874 mm. A particular reason for selecting the catchment was the relatively frequent occurrence of debris flows: 146 in the period 1956–2001 (Lorente *et al*., 2003; Beguería, 2006).

The original model parameterization and calibration are described by Bathurst *et al*. (2007). Using a 10-m resolution DEM, the SHETRAN grid was discretized with a 500-m resolution and the landslide-model sub-grid resolution was set at 20 m. Spatial variability was modelled in overland flow resistance, evapotranspiration and root cohesion as a function of vegetation (three types) and in soil hydraulic and geotechnical properties as a function of soil texture (two textures). Soil depth was uniform at 1·5 m, and parameters were adjusted during the calibration process as in the Valsassina application. For a 4-year simulation period, using data from rain gauges at Bescos in the catchment and at Jaca, the hydrological component was calibrated against regionally derived discharge data (including normalized flow duration curves). The landslide component was tested against an inventory map of landslide occurrence in the catchment (compiled for 1956–2001), showing an ability to represent the observed spatial pattern. The sediment transport and yield component were again calibrated against regional data.

Analysis of debris flow characteristics in the flysch sector of the Spanish Pyrenees quantified the mean value of the critical hillslope below which debris flow deposition starts to occur as 18° and the run-out distance as 60% of the difference in elevation between the landslide location and the critical slope (Lorente *et al*., 2003). These values therefore replaced the SHETRAN default values of 10° and 40% (Burton and Bathurst, 1998) for the Ijuez application.

In both applications, the landslide-model sub-grid resolution of 20 m is potentially larger than typical shallow landslide dimensions but is constrained by the available DEM resolution. In the area of the Ijuez catchment, for example, landslide widths have been measured in the range 7·4–30 m (mean about 15 m) (Lorente *et al*., 2003). It is acknowledged that the model may therefore not entirely represent local topographic controls on shallow landsliding. This, and other, scale issues are a source of uncertainty in the simulations, discussed in some detail by Bathurst *et al*. (2006). The means of allowing for this uncertainty are explained in the section on Uncertainty below.

METHODOLOGY

The following methodology was developed to relate the magnitude of a landsliding event (quantified as the number of shallow landslides occurring) to the frequency of occurrence represented by the rainfall-event return period and to establish the magnitude of the impact in terms of sediment yield at the catchment outlet:

1. Create SHETRAN models of each focus catchment, for hydrology, landslide occurrence and sediment yield. In this case the models were already created and calibrated in the original applications to the Valsassina-Esino and Ijuez catchments (Bathurst *et al*., 2005, 2007).
2. Generate rainfall events of different magnitude (i.e. intensities of different return period) for a range of durations (1-day to 5-day) for each focus area
3. Apply these events to the SHETRAN model to give numbers of shallow landslides triggered and the resulting sediment yield
4. Analyse the results graphically for relationships between rainfall intensity, rainfall duration and landslide numbers and sediment yield.

Generation of rainfall events for different return periods

Using existing records, rainfall events were generated for 1-, 2-, 3-, 4- and 5-day durations, each for a range of return periods of 2 years and greater. This provided the basis for exploring the relationship between landslide magnitude and rainfall intensity and duration. The three main steps in the procedure were the production of rainfall frequency curves based on daily data, disaggregation of the daily rainfall into the hourly values required as input to SHETRAN and representation of the appropriate spatial distribution in each catchment.

Daily rainfall data were available for five sites within the Valsassina catchment, for periods of 21, 29, 32, 34 and 44 years respectively. Within the Ijuez catchment, daily

Copyright © 2011 John Wiley & Sons, Ltd.

rainfall data were available at only one site (Bescos), for a total of 23 years. Additional data were available at two neighbouring sites within 10 km of the catchment (for periods of 20 and 31 years).

For the 1-day duration event, the annual maximum 1-day rainfalls were extracted from each data set, then ranked and a generalized extreme value (GEV) distribution was fitted using L-moments. The resulting frequency curve gives the amount of rainfall expected in 1 day at the gauge location as a function of return period. The procedure was repeated for the 2-, 3-, 4- and 5-day duration events and Figure 2 presents Gumbel plots with examples of the goodness of fit achieved. Rainfall events were generated for return periods of 2, 5, 10, 25 and (for Valsassina only) 50 years. Given the maximum lengths of the rainfall records, the frequency curves for return periods greater than about 20–25 years (Valsassina) and 10–15 years (Ijuez) are likely to be more uncertain because of the lack of data constraining the fit. The difficulties of defining return periods for high magnitude rainfalls in mountain areas are highlighted by García-Ruiz *et al*. (2000). They include not only inadequate record lengths but inadequate spatial density of sampling, lack of sub-daily rainfall records, only partial dependency of rainfall on relief and large spatial variability in return periods of given rainfall.

SHETRAN requires precipitation input at the hourly time scale, so the daily (or multiple day) rainfall totals were disaggregated into hourly intervals. However, the temporal distribution of rainfall within a day at the focus sites is variable and cannot be characterized by a single pattern. Crosta and Frattini (2001) identified two different rainfall patterns for northern Italy, each leading to significant landslide events: single burst events characterized by short duration, high-intensity rainfall and multiple burst events of longer duration but lower intensity. If the study of the impacts of rainfall on shallow landsliding is to be representative, at least some of this variability should be taken into account. Four different hourly rainfall distribution patterns were therefore generated, having different hourly intensities but the same total precipitation in the same period (Tables I and II). Figure 3 shows an example of the patterns for the 1-day event for the Valsassina catchment. The 'central-peak' hourly rainfall distribution is a symmetrical variation rising from zero at the start of the period to a maximum in the middle of the period and falling to zero at the end of the period. The 'constant' distribution is a steady low-intensity rainfall throughout the period. The 'early peak' distribution has its highest rainfall intensity at the start of the period, followed by a linear decrease in rainfall throughout the rest of the period, whereas the 'late peak' distribution has the opposite pattern, with its highest rainfall intensity at the end of the period. A Newcastle University rainfall disaggregation code, Raindist (Kilsby, personal communication), was modified and used to generate the chosen distributions. The distributions represent a compromise between simulating a wide range of single-peak rainfall distributions and minimizing the number of simulations. They contrast high-intensity rainfall of short duration and low-intensity rainfall of long duration and they maximize the differences due to timings of the peak rainfall (and thereby allow antecedent rainfall effects to be explored). The different rainfall patterns also enable the temporal occurrence of landslides to be explored, an aspect which has received little attention in previous modelling studies.

For the Valsassina catchment, the preceding procedure was followed for each of the five raingauges in the catchment and the spatial distribution of rainfall was calculated using Thiessen polygons. (An altitude dependency was not evident from the available data and was therefore not modelled.) For the Ijuez catchment, only one raingauge lies within the catchment but spatial variation was represented by three altitudinal bands, on the basis of an altitude dependency in annual rainfall determined from local regional data (Bathurst *et al*., 2007).

Model runs

Each generated rainfall event was applied in turn to the relevant catchment. A total run time of 3 months was simulated in each case, consisting of a 'settling down' period of 1 month before the actual event and a 2-month 'follow-up' period for simulating the impact of the event. No rain was applied during the settling down and follow-up periods. Both catchments were simulated with minimum levels of evapotranspiration, set to average levels for January–March. The initial phreatic surface level was set at a depth of 1 m but then allowed to adjust (improving consistency between grid squares) during the settling down period. The resulting river flows were relatively high for the Valsassina catchment (corresponding to discharges typical of autumn/winter) but rather lower for the Ijuez catchment (corresponding to conditions typical of a dry summer). These settings effectively defined the antecedent soil moisture conditions for the event: the impact of different antecedent conditions on the simulation results was not investigated (except through the application of different rainfall events) but is recognized as an important topic for any follow-up study, as highlighted by Frattini *et al*. (2009). Simulations (with the hydrology, erosion and sediment yield components) were run both with and without the landslide component, in order to determine the sediment yield attributable to landslides.

Simulation output for each event consisted of the number of shallow landslides triggered (equal to the number of model sub-grid elements in which a landslide is simulated), the time of occurrence and the spatial location of each landslide, identification of which landslides evolved into debris flows and the overall catchment-scale sediment yield. The latter was determined for a period of 1 month from the start of the rainfall, a duration which was chosen arbitrarily but which was considered long enough to account for the full event response.

Uncertainty

It is generally acknowledged that the parameterization of physically based, spatially distributed models involves

Copyright © 2011 John Wiley & Sons, Ltd.

Table I. Event rainfall (mm) for the Valsassina catchment (rainfall for Bellano)

		Central-peak rainfall event					Constant rainfall					Early/late peak				
		Return period (years)					Return period (years)					Return period (years)				
		2	5	10	25	50	2	5	10	25	50	2	5	10	25	50
Total (mm)	1-day event	77·5	108·9	130·9	160·1	182·9	77·5	108·9	130·9	160·1	182·9	77·5	108·9	130·9	160·1	182·9
	2-day event	109·1	143·3	163·0	185·1	199·6	109·1	143·3	163·0	185·1	199·6	109·1	143·3	163·0	185·1	199·6
	3-day event	123·9	158·9	179·2	201·9	217·0	123·9	158·9	179·2	201·9	217·0	123·9	158·9	179·2	201·9	217·0
	4-day event	135·3	171·9	192·9	216·3	231·7	135·3	171·9	192·9	216·3	231·7	135·3	171·9	192·9	216·3	231·7
	5-day event	141·4	177·3	198·5	222·8	239·1	141·4	177·3	198·5	222·8	239·1	141·4	177·3	198·5	222·8	239·1
Max (mm/h)	1-day event	14·8	20·7	24·9	30·5	34·8	3·2	4·5	5·5	6·7	7·6	5·9	8·4	10·0	12·3	14·0
	2-day event	10·5	13·8	15·7	17·8	24·5	2·3	3·0	3·4	3·9	4·2	4·4	5·7	6·5	7·4	8·0
	3-day event	8·0	10·2	11·5	13·0	13·9	1·7	2·2	2·5	2·8	3·0	3·3	4·3	4·8	5·5	5·9
	4-day event	6·5	8·3	9·3	10·4	11·2	1·4	1·8	2·0	2·3	2·4	2·8	3·5	3·9	4·4	4·7
	5-day event	5·5	6·9	7·7	8·6	9·2	1·2	1·5	1·7	1·9	2·0	2·3	2·9	3·3	3·7	3·9
Mean (mm/h)	1-day event	3·2	4·5	5·5	6·7	7·6	3·2	4·5	5·5	6·7	7·6	3·2	4·5	5·5	6·7	7·6
	2-day event	2·3	3·0	3·4	3·9	4·2	2·3	3·0	3·4	3·9	4·2	2·3	3·0	3·4	3·9	4·2
	3-day event	1·7	2·2	2·5	2·8	3·0	1·7	2·2	2·5	2·8	3·0	1·7	2·2	2·5	2·8	3·0
	4-day event	1·4	1·8	2·0	2·3	2·4	1·4	1·8	2·0	2·3	2·4	1·4	1·8	2·0	2·3	2·4
	5-day event	1·2	1·5	1·7	1·9	2·0	1·2	1·5	1·7	1·9	2·0	1·2	1·5	1·7	1·9	2·0
Mean (mm/day)	1-day event	77·5	108·9	130·9	160·1	182·9	77·5	108·9	130·9	160·1	182·9	77·5	108·9	130·9	160·1	182·9
	2-day event	54·6	71·6	81·5	92·5	99·8	54·6	71·6	81·5	92·5	99·8	54·6	71·6	81·5	92·5	99·8
	3-day event	41·3	53·0	59·7	67·3	72·3	41·3	53·0	59·7	67·3	72·3	41·3	53·0	59·7	67·3	72·3
	4-day event	33·8	43·0	48·2	54·1	57·9	33·8	43·0	48·2	54·1	57·9	33·8	43·0	48·2	54·1	57·9
	5-day event	28·3	35·5	39·7	44·6	47·8	28·3	35·5	39·7	44·6	47·8	28·3	35·5	39·7	44·6	47·8

Copyright © 2011 John Wiley & Sons, Ltd.

Copyright © 2011 John Wiley & Sons, Ltd.

Table II. Event rainfall (mm) for the Ijuez catchment (rainfall for the 800–1200 m altitude band)

		Central-peak rainfall event				Constant rainfall				Early/late peak			
		Return period (years)				Return period (years)				Return period (years)			
		2	5	10	25	2	5	10	25	2	5	10	25
Total (mm)	1-day event	57·2	69·7	76·7	84·3	57·2	69·7	76·7	84·3	57·2	69·7	76·7	84·3
	2-day event	69·6	86·4	98·2	113·9	69·6	86·4	98·2	113·9	69·6	86·4	98·2	113·9
	3-day event	84·1	105·2	118·3	133·9	84·1	105·2	118·3	133·9	84·1	105·2	118·3	133·9
	4-day event	91·0	114·3	129·7	148·9	91·0	114·3	129·7	148·9	91·0	114·3	129·7	148·9
	5-day event	99·1	122·9	136·7	152·1	99·1	122·9	136·7	152·1	99·1	122·9	136·7	152·1
Max (mm/h)	1-day event	12·0	14·6	16·1	17·6	2·4	2·9	3·2	3·5	4·8	5·8	6·5	7·2
	2-day event	7·4	9·1	10·3	12·0	1·5	1·8	2·0	2·4	3·1	3·9	4·3	5·1
	3-day event	5·9	7·5	8·4	9·5	1·2	1·5	1·6	1·9	2·5	3·1	3·5	4·0
	4-day event	4·8	6·1	6·9	7·9	0·9	1·2	1·4	1·6	2·1	2·5	2·9	3·3
	5-day event	4·2	5·2	5·8	6·5	0·8	1·0	1·1	1·3	1·8	2·2	2·4	2·8
Mean (mm/h)	1-day event	2·4	2·9	3·2	3·5	2·4	2·9	3·2	3·5	2·4	2·9	3·2	3·5
	2-day event	1·5	1·8	2·0	2·4	1·5	1·8	2·0	2·4	1·5	1·8	2·0	2·4
	3-day event	1·2	1·5	1·6	1·9	1·2	1·5	1·6	1·9	1·2	1·5	1·6	1·9
	4-day event	0·9	1·2	1·4	1·6	0·9	1·2	1·4	1·6	0·9	1·2	1·4	1·6
	5-day event	0·8	1·0	1·1	1·3	0·8	1·0	1·1	1·3	0·8	1·0	1·1	1·3
Mean (mm/day)	1-day event	57·2	69·7	76·7	84·3	57·2	69·7	76·7	84·3	57·2	69·7	76·7	84·3
	2-day event	34·8	43·2	49·1	56·9	34·8	43·2	49·1	56·9	34·8	43·2	49·1	56·9
	3-day event	28·0	35·1	39·4	44·6	28·0	35·1	39·4	44·6	28·0	35·1	39·4	44·6
	4-day event	22·8	28·6	32·4	37·2	22·8	28·6	32·4	37·2	22·8	28·6	32·4	37·2
	5-day event	19·8	24·6	27·3	30·4	19·8	24·6	27·3	30·4	19·8	24·6	27·3	30·4

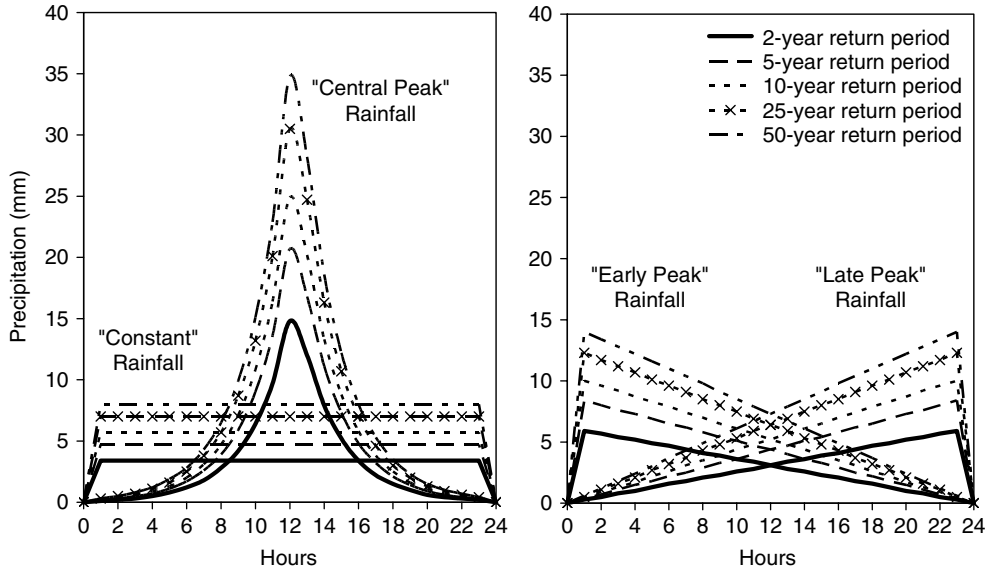

Figure 3. Example of the simulated 1-day rainfall patterns for different return periods for the Bellano gauge, Valsassina catchment

uncertainty (e.g. Beven and Binley, 1992; Beven, 2001, 19–23; Guimarães *et al*., 2003), one potentially important source being inconsistencies between the model grid scale, the scale at which property measurements are made and the scale relevant to each particular hydrological process (e.g. saturated conductivity is measured at the scale of an auger hole but the model grid scale may be tens to hundreds of metres). This uncertainty creates the potential for multiple parameterizations with possibly quite different but apparently equally acceptable combinations of parameter values. It is therefore also accepted that the uncertainty and its implications for model output should be explicitly recognized in the modelling procedure (e.g. Beven and Binley, 1992; Ewen and Parkin, 1996). Typically this is achieved by quantifying some form of uncertainty envelope. The original simulations therefore established upper and lower uncertainty bounds on the output as a function of uncertainty in key model parameters. For example, bounds on landslide occurrence were determined as a function of vegetation root cohesion. For the research reported here, though, (simply developing and testing a hazard prediction method) it was sufficient to use a single parameter set to characterize each catchment. The selected sets are those used to produce the lower bounds for landslide occurrence in the original simulations, which approximate the measured annual rates of landsliding. The corresponding root cohesions were: for the Valsassina catchment, 7500 Pa for forest cover and 3500 Pa for pasture; and for the Ijuez catchment, 1500 Pa for natural pine forest and 800 Pa for pine plantation, shrubs and meadows. These values are based on such literature sources as Preston and Crozier (1999), Sidle *et al*. (1985, p62) and Sidle and Ochiai (2006, 103–104).

Because of the impracticality of measuring the required landslide-model parameters (for the factor-of-safety equation) at every model sub-grid square across the entire catchment, there is a reliance on estimated values. A certain proportion of squares is then characterized with unrealistic combinations of parameter values and is simulated to be unconditionally unstable, even in dry conditions. Eliminating these and taking into account also those landslide squares which were determined to be stable for all conditions, the maximum numbers of squares at which the model could simulate landslides were 285 and 94 for the Valsassina and Ijuez catchments respectively.

ANALYSIS AND DISCUSSION OF RESULTS

Comparison of observed and generated rainfall return periods for landsliding events

As noted earlier, the generated rainfall events have the same total precipitation but different hourly intensities in the same period, depending on the sub-daily rainfall distribution (Tables I and II). A distinction should therefore be made between return periods based on daily events (as defined here) and the return period of hourly events which, in this study, are variable. The distinction is important since shallow landslides are typically triggered by short intense bursts of rainfall of even less than hourly duration within longer periods of rainfall (e.g. Dhakal and Sidle, 2004; Sidle and Ochiai, 2006, p69). Therefore, it needs to be shown that the generated daily (or longer period) rainfalls and their sub-daily distributions produce landsliding events in a manner comparable with observation and that the return periods of the generated rainfalls similarly match the observed return periods. The limited availability of data permits only one such comparison, for the 26 to 27 June 1997 storm event in the Esino-Valsassina area recorded by Frattini *et al*. (2009). In less than 2 h almost 100 mm of rain (i.e. an intensity of nearly 50 mm h^{-1}) triggered 147 shallow landslides within an area of 40 km^2 (i.e. 3·7 landslides per square kilometre). The associated 1-day rainfall was 168 mm. The return

Copyright © 2011 John Wiley & Sons, Ltd.

period for the 2-h rainfall is 75 years, while the return period for the daily rainfall, according to Figure 2, is more than 50 years. (The uncertainty is too great in this portion of the curve to determine an accurate value.) For comparison, Tables I and III present the necessary data on the generated rainfall events and the numbers of landslides for the central-peak rainfall distribution as a function of rainfall return period and rainfall event duration. The 1-day rainfall for a 50-year return period is 183 mm, with a peak intensity of 35 mm h^{-1}; this triggers 207 landslides over the 180-km^2 simulation area event (i.e. 1 landslide per square kilometre). These figures show excellent order of magnitude agreement with the observations and suggest that it is possible to define rainfall return periods at the daily scale that, with the central-peak distribution, can adequately represent the storm events that generate landslides in the Valsassina region.

Nevertheless, the simulation data also show that a 1-day event with a 10-year return period is sufficient to trigger most of the above landslides, i.e. a 1-day rainfall of 131 mm with a peak intensity of 25 mm h^{-1} still generates 196 landslides. Similarly, a 5-day event with a 10-year return period providing 199 mm of rainfall (i.e. a mean daily rainfall of 40 mm) with a peak intensity of 7·7 mm h^{-1} generates 226 landslides. Lack of observations means that it is not possible to confirm if shorter return period events can, in reality, trigger such substantial levels of landsliding. However, some support is provided by Luino's (2005) observation for the same area that slope instabilities begin once the cumulative event rainfall exceeds approximately 10% of the local mean annual rainfall. On the basis of the Bellano annual total of 1240 mm noted earlier, an event total of 120 mm or more would therefore be expected to cause landslides.

Table III. Number of landslides simulated for the central-peak rainfall pattern for the Valsassina and Ijuez catchments

Valsassina					
	Number of landslides for events of duration (day)				
Return period (year)	1	2	3	4	5
2	109	159	167	169	175
5	147	204	208	210	214
10	196	210	224	225	226
25	207	218	231	237	237
50	207	233	237	237	237

Ijuez					
	Number of landslides for events of duration (day)				
Return period (year)	1	2	3	4	5
2	87	90	94	94	94
5	94	94	94	94	94
10	94	94	94	94	94
25	94	94	94	94	94

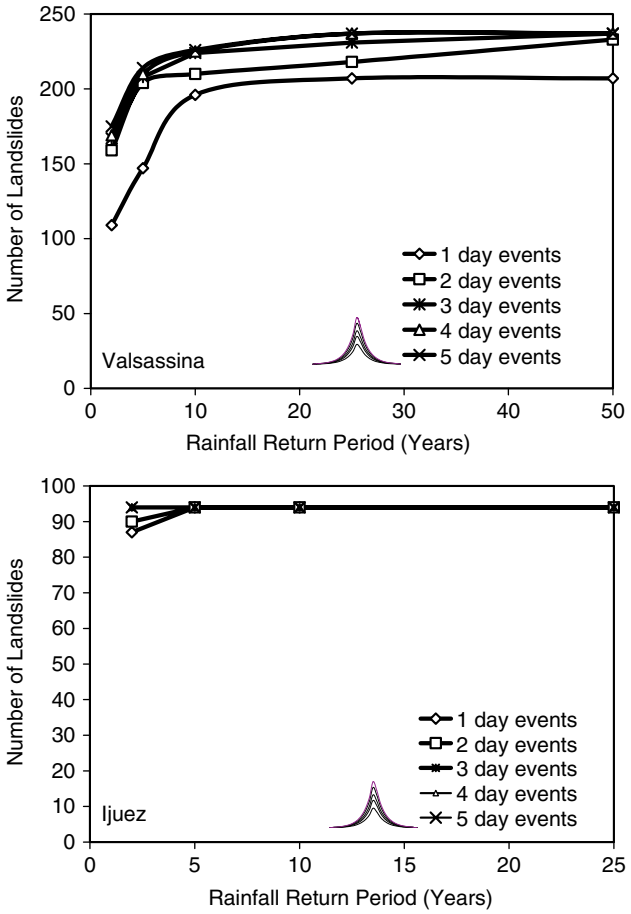

Figure 4. Relationship between the number of landslides and rainfall return period for different event durations, for the central-peak rainfall distribution, for the Valsassina and Ijuez catchments

Comparison of this threshold with the data in Table I suggests, then, that 3-, 4- and 5-day events with a 2-year return period and 1- and 2-day events with return periods of less than 10 years should produce landslides. That is, it would seem that rainfalls with short return period can be associated with landslides.

Relationship between central-peak daily rainfall return period and landsliding magnitude

Figure 4 complements Table III in showing numbers of landslides for the central-peak rainfall distribution as a function of rainfall return period and rainfall event duration. A striking feature, for a given event duration, is the insensitivity of simulated landslide magnitude to return period for return periods greater than about 10 years for the Valsassina catchment and 5 years for the Ijuez catchment. In the latter case the number of landslides quickly reaches 94, the maximum possible, while in the Valsassina catchment the number asymptotes to 237, which is less than the maximum possible (285). Similarly, for an event of given return period, landslide magnitude becomes less sensitive to event duration as duration increases. The results may be interpreted in terms of the model design as follows.

For the Valsassina catchment a similar pattern has been obtained by Frattini *et al.* (2009) using a different but

Copyright © 2011 John Wiley & Sons, Ltd.

still physically based model. Those authors suggest an explanation whereby, as rainfall intensity increases, landsliding in effect becomes limited by the rate at which rain can infiltrate into the soil. For the SHETRAN simulations, though, apart from a few cases, rainfall intensities are generally less than the soil saturated conductivity. A more likely explanation for the simulated pattern in this case, is that, for each rainfall duration, the soil in the critical areas is already simulated to be saturated by the events with approximately 10-year return periods, thus producing the maximum number of landslides from those areas. Within the model, the additional rainfall from larger events generates surface runoff and does not affect the porewater pressures responsible for landsliding. It may be queried, though, why the maximum number of simulated landslides asymptotes to a value (237) which is less than the maximum possible number (285), i.e. Why does the additional rainfall of the higher return period events not cause any of the remaining squares to fail? The answer appears to be that the non-failing landslide squares are concentrated in just six SHETRAN grid squares (with the majority in only three squares). These squares are all on the edge of the simulation area or at a catchment watershed (or divide) with no uphill contributing area. It is likely, therefore, that, within the simulations, these few squares have just the necessary characteristics to allow rapid drainage of the soil column for the applied rainfalls, thus preventing the occurrence of the necessary porewater conditions to trigger slope failure, i.e. it is the result of the way in which the catchment is represented in the model.

For the Ijuez catchment, rainfalls with relatively low recurrence intervals are sufficient, in the simulation, to trigger the maximum possible number of landslides; larger rainfalls can then have no additional effect. This pattern is consistent with the observation of Lorente *et al*. (2003) that the triggering of shallow landslides and the subsequent formation of debris flows in the Ijuez catchment is related to relatively frequent intense rainfalls with recurrence intervals of no more than 2–5 years. However, it may be queried if the maximum number of landslides possible (94) is realistic. Within the model, this maximum is a function of the selected root cohesion values and the number of unconditionally unstable sub-grid elements (which are eliminated from consideration). Root cohesion varies spatially with vegetation type but, within the model, is constant for each individual type, thereby reducing the scope for representing local variation in landslide susceptibility. Likewise, limited ability to represent local variations in soil depth, elevation and other characteristics may result in too many sub-grid elements being designated as unconditionally unstable. Further research into sensitivity to parameter evaluation and into model refinement is necessary to address this point.

It is likely that the pattern of landslide numbers showing progressive insensitivity as the rainfall event increases to extreme levels has been exaggerated in the simulations as a result of the model characteristics. Nevertheless, such behaviour is not physically unrealistic, although not necessarily typical of all catchments. The only example found in the literature is from North Island, New Zealand, which is admittedly a different physical context from the mountain chains of the Alps and Pyrenees: Reid and Page (2002), in their Figure 6, present data-based convex-upwards curves relating areal landslide frequency (i.e. number of slides per square kilometre per year) to storm recurrence interval for the Waipaoa catchment. Their observation that 50% of landslides occur in storms with return periods of less than 8 years, while raising the occurrence to 75% requires storms with return periods of up to 27 years, fits the pattern of decreasing sensitivity.

Effect of temporal distribution of rainfall

The simulation results for the four within-event rainfall distributions are compared in Figures 5–7. Figure 5 repeats Figure 4 but shows the effects of the different distributions. For reasons of clarity, results are shown for only the 1-day duration events but the general pattern is the same for all the durations. For a given event, the rainfall total is the same but the temporal distribution varies as shown in Figure 3. Figure 6 provides hydrological context by comparing the catchment outlet discharges associated with the different patterns for a 1-day rainfall event with a 2-year return period. For the same event, Figure 7 shows the numbers of landslides occurring as a function of time through the event and relative to the outlet discharge hydrograph. For both catchments, the 'central-peak' and 'constant' rainfall patterns produce almost the same numbers of landslides and thus similar curves in Figure 5. However, the hydrological response and the incidence of landsliding differ between the patterns and between the catchments. For the Valsassina catchment, the central-peak rainfall pattern produces a flashy, high peak discharge response, while the constant rainfall pattern produces a more moderate, lower discharge response (Figure 6). More landslides tend to occur earlier with the central-peak rainfall and later with the constant rainfall (following a build-up of critical conditions) (Figure 7). For the Ijuez catchment, the constant rainfall pattern produces a higher peak discharge than the central-peak rainfall pattern but with a greater delay (Figure 6). In both cases, the occurrence of landslides is delayed relative to the timings for the Valsassina catchment (Figure 7). The differences between the catchments may be explained by the drier soil conditions in the Ijuez catchment absorbing more of the rainfall and delaying both landslide occurrence and stormflow response.

The 'early peak' and 'late peak' rainfall patterns produce somewhat similar curves in Figure 5 but dissimilar responses in Figures 6 and 7. Both produce lower numbers of landslides than the central-peak and constant patterns. It is perhaps not surprising that the central-peak pattern produces more landslides as its peak rainfall intensity is significantly higher than those of the other two.

Copyright © 2011 John Wiley & Sons, Ltd.

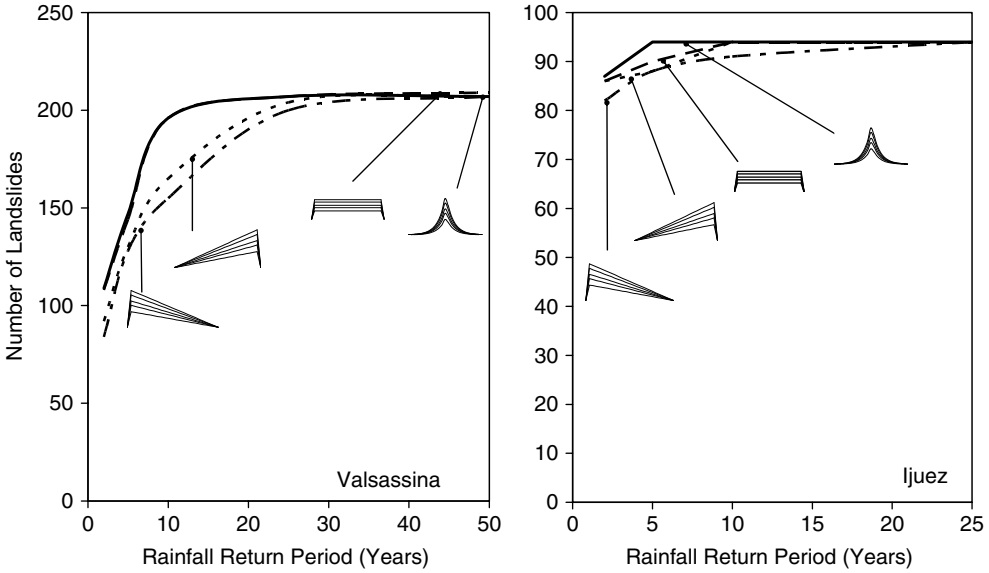

Figure 5. Relationship between the number of landslides and rainfall return period for the 1-day duration events, for the four rainfall patterns (shown diagrammatically), for the Valsassina and Ijuez catchments

That the constant pattern should also produce more landslides, though, suggests that the effects of the higher peak intensities of the early and late peak patterns are more than compensated for by the constant rainfall intensity exceeding the other two intensities for half the period (Figure 3). In the case of the early peak, much of the initial higher rainfall is likely to have been absorbed in the relatively dry soil. Landslides are triggered in some quantity after the rainfall peak and continue at a lesser rate as rainfall (and soil moisture) declines. In the case of the Ijuez, the peak discharge is not generated until after the peak discharge for the central-peak case, again indicating variations in the interaction between time-varying rainfall intensity and soil moisture conditions. In the case of the late peak pattern, the steady build-up of rainfall starting from zero allows the early moisture to drain without causing significant landsliding, thus blunting the impact of later increases in soil moisture. However, landsliding begins before the peak rainfall occurs and continues for some time later. In the Ijuez, these variations are again delayed because of the drier soil conditions and are more muted since, once the maximum number of landslides has occurred, there can be no further time variation of landslide numbers.

Past studies refer to landslides occurring during a rainfall event but the simulations show also a significant number of landslides occurring after the rain has stopped (Figure 7). These are considered to be the result, within the model, of subsurface downslope transfers of water creating the critical saturation (or porewater pressure) conditions in the soil column. Field data on the temporal occurrence of landslides through an event are rare and at

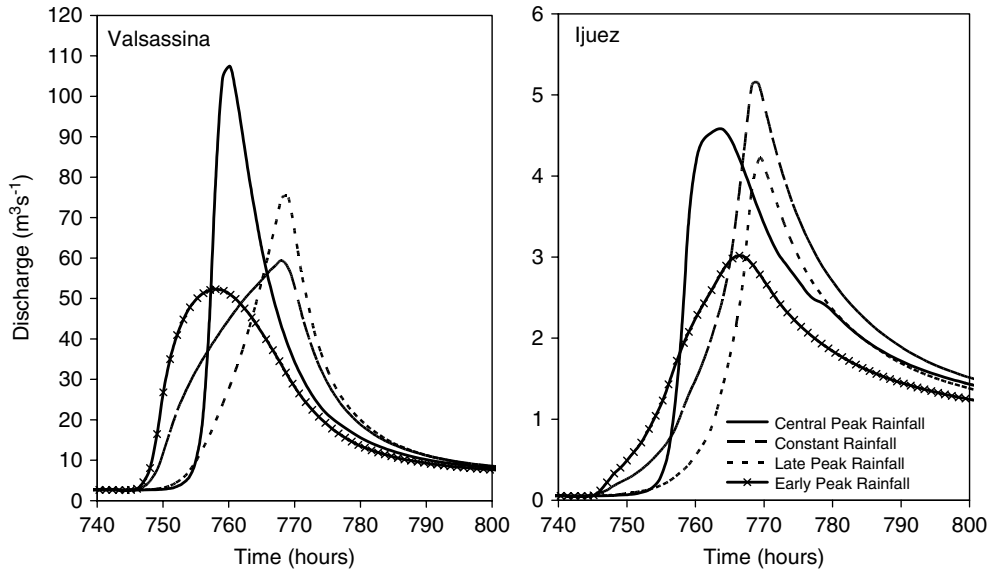

Figure 6. Comparison of discharges simulated at the outlets of the Valsassina and Ijuez catchments for the four rainfall patterns. The examples are for a 1-day rainfall event with a 2-year return period

Copyright © 2011 John Wiley & Sons, Ltd.

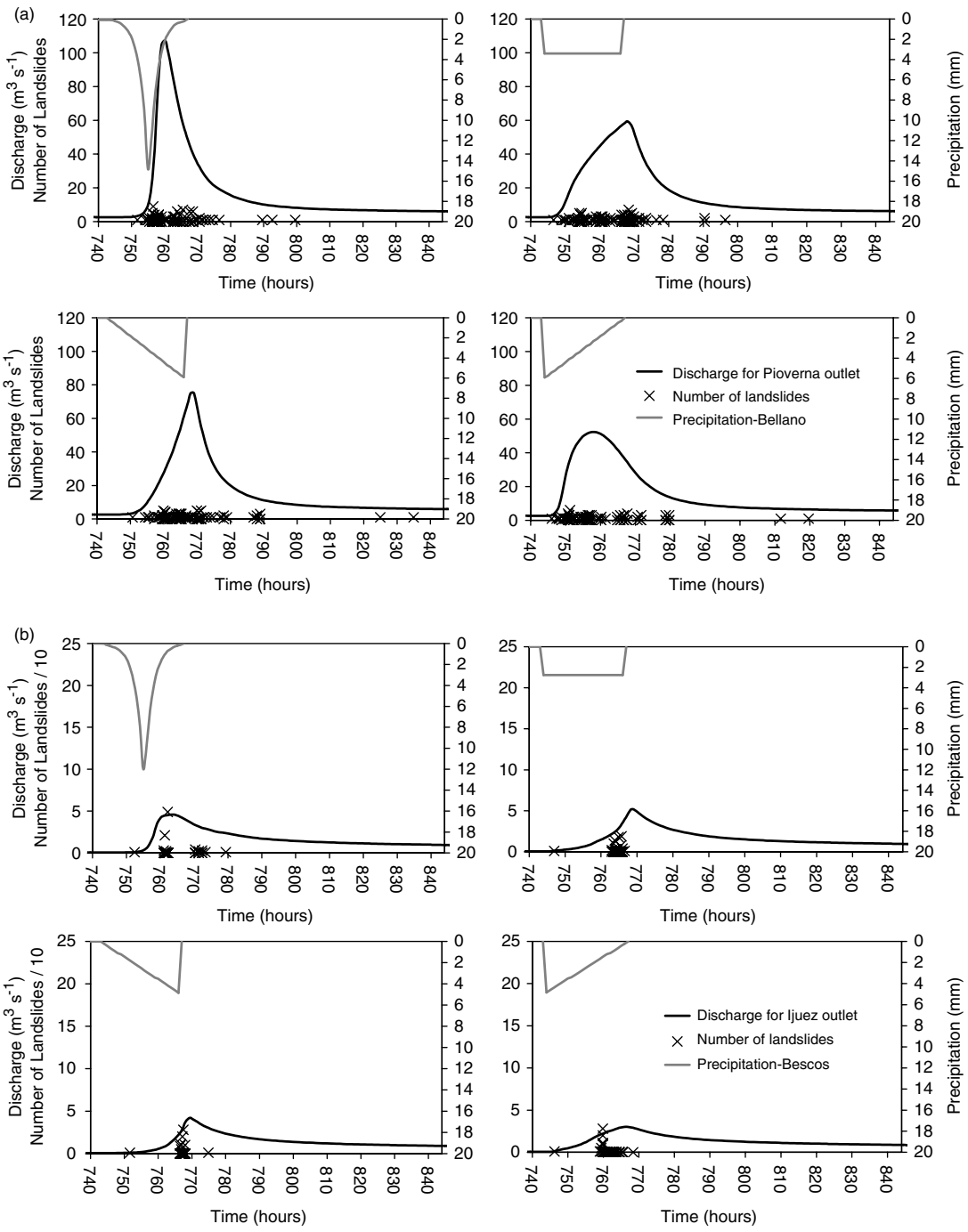

Figure 7. Outlet discharge hydrographs and time variation of landslide occurrence for the four rainfall patterns. Results are shown for the Valsassina (a) and Ijuez (b) catchments for a 1-day event with a 2-year return period. Each cross indicates the number of landslides occurring at a specific simulation time

present it is not clear whether such post-rain failures are likely to occur in practice or whether the model has highlighted an interesting but not very typical phenomenon. However, Chen *et al*. (2005) report the temporal occurrence of 39 debris flows caused by typhoons and other major rainfall events hitting Taiwan. In 16 cases, debris flows occurred prior to the peak hourly rainfall; 10 cases occurred at the time of peak hourly rainfall and 13 cases occurred after the peak rainfall.

The simulation results described above show that the temporal distribution of rainfall in an event can have a significant effect on the potential number of landslides. For an event of given duration and return period, high-intensity central-peak rainfalls and constant low-intensity rainfalls seem to cause the maximum number of landslides, despite variations in catchment hydrological response and in the timing of landslide occurrence.

Cumulative and antecedent precipitation has a large influence on soil moisture conditions and affects the type and timing of landslide occurrence. Although the Valsassina and Ijuez hydrological responses to the various rainfall events differ (Figure 6) and their initial soil

Copyright © 2011 John Wiley & Sons, Ltd.

moisture conditions also differ (dry summer conditions for Ijuez and autumn conditions for Valsassina), the simulations show that, for events of a given return period, the majority of landslides occur at timings related more to the rainfall distribution pattern than to other factors such as catchment characteristics. A similar time distribution of landslides occurs in both catchments as a function of the rainfall distribution pattern.

Volume of sediment reaching the river network

The volume of landslide material delivered to the channel network depends on the number of landslides which evolve into hillslope debris flows, the number of those debris flows which connect directly with the channel system and the amount of material which is either lost from the debris flow through deposition in the run-out zone before the debris flow reaches the river or added through scour along the debris flow path. (The model allows for a part of the deposited material to be subsequently washed into the channel by overland flow. As noted earlier, though, the option to allow additional scour was not exercised at the focus sites.) Its contribution to the sediment yield at the catchment outlet then depends on the routing of the material along the channel network (as a conventional sediment load) as a function of timing of the sediment injection and the discharge hydrograph. Total sediment yield also depends on material from other sources, limited in the model to soil eroded by raindrop impact and overland flow and to sediment already in the channel bed. For the Valsassina catchment only one debris flow from the 285 maximum possible landslides could potentially reach the channel network. This means that 0·35% of landslides have the potential for some part of their material to be deposited into the channel network. For a 5-day, 50-year return period event, the simulated event sediment yield without any landslide contribution (i.e. from erosion by raindrop impact and overland flow plus transport of sediment already in the channel bed) is 31 960 t, while the total event sediment yield including the landslide contribution is 32 202 t. The landslide sediment yield at the catchment outlet is therefore 242 t or 0·75% of the total event sediment yield. A possible explanation for this seemingly rather low figure is that the channel network is represented with too coarse a resolution to include the low-order streams which, in reality, may be adjacent to landslide sites and thus allow more debris flows to reach the channel network. It should be remembered also that the debris flows referred to here are hillslope flows; the model does not represent debris flows which develop within the channels.

Similarly, for the Ijuez catchment, 13 debris flows from the 94 maximum possible landslides could potentially reach the channel network, meaning that 13·8% of landslides have the potential for some part of their material to be deposited into the channel. For a 5-day, 25-year return period event, the simulated event sediment yield without any landslide contribution is 3520 t, while the total event sediment yield including the landslide contribution is 5050 t. The landslide sediment yield at the catchment outlet is therefore 1530 t or 30% of the total event sediment yield. The greater contribution in the Ijuez catchment relative to the Valsassina catchment is likely to be the result of a greater presence of steep slopes near the channel network and thus a greater potential for debris flows to reach the network. That is, the Ijuez is more of a headwater catchment with greater landslide connectivity.

The few available field surveys show similarly that the capacity of hillslope debris flows to deliver material to the channel network varies widely. Reid and Page (2002) found that, for debris flows generated during a major cyclone in an unspecified sub-catchment of the Waipaoa catchment in New Zealand, 35% of debris flows did not reach the channel network, 40% of debris flows travelled down a hillslope before depositing some sediment in a channel and 25% of landslides abutted a channel and delivered all their sediment. The overall sediment delivery ratio from shallow landslides was estimated to be 45%. Page *et al*. (2004) similarly calculated that the long-term (114 years) delivery ratio for landslide-derived sediment in the Tutira catchment was 43%. Imaizumi and Sidle (2007), for the Miyagawa Dam catchment in Japan, found that the percentages of landslides delivering some part of their material to channels varied from 56 to 75% in a 35-year period and that they were correlated with maximum hourly rainfall. They suggest that debris flow mobility varies as a function of water content in both initially failed material and transported sediment. At a smaller scale of landslide, Johnson *et al*. (2000) in a survey in southeastern Alaska found many examples of landslides or debris flows contributing sediment directly to channels (especially first and second-order streams), including one that deposited over 100 m^3 of sediment and woody debris.

Figure 8 shows the total event sediment yield simulated at both catchment outlets as a function of rainfall event, event duration and event return period for the central-peak rainfall distribution. For comparison, the yield simulated without landslides is also shown (labelled 'no landslides' in the figure). For the Valsassina catchment, only one debris flow can reach the channel and landslides add little to the overall sediment yield; the two sets of curves therefore more or less coincide. For the Ijuez catchment, the landslides increase sediment yield by 0–71%.

There are few data in the literature with which the simulated sediment yield data and the relationships of Figure 8 can be compared. It is evident, though, that the contribution of landslides to total sediment yield can vary widely even in the same catchment. From two studies in New Zealand, Hicks *et al*. (2000) found that shallow landslides generated most of the sediment supply to the stream network in the 83 km^2 Te Arai catchment (lower tributary to the Waipaoa), while Reid and Page (2002) calculated that shallow landslides contribute about 15% of the annual suspended sediment yield exported by the upper Waipaoa river catchment (1580 km^2). A diagram in the field notes for the 6th Gravel-bed Rivers Conference

Copyright © 2011 John Wiley & Sons, Ltd.

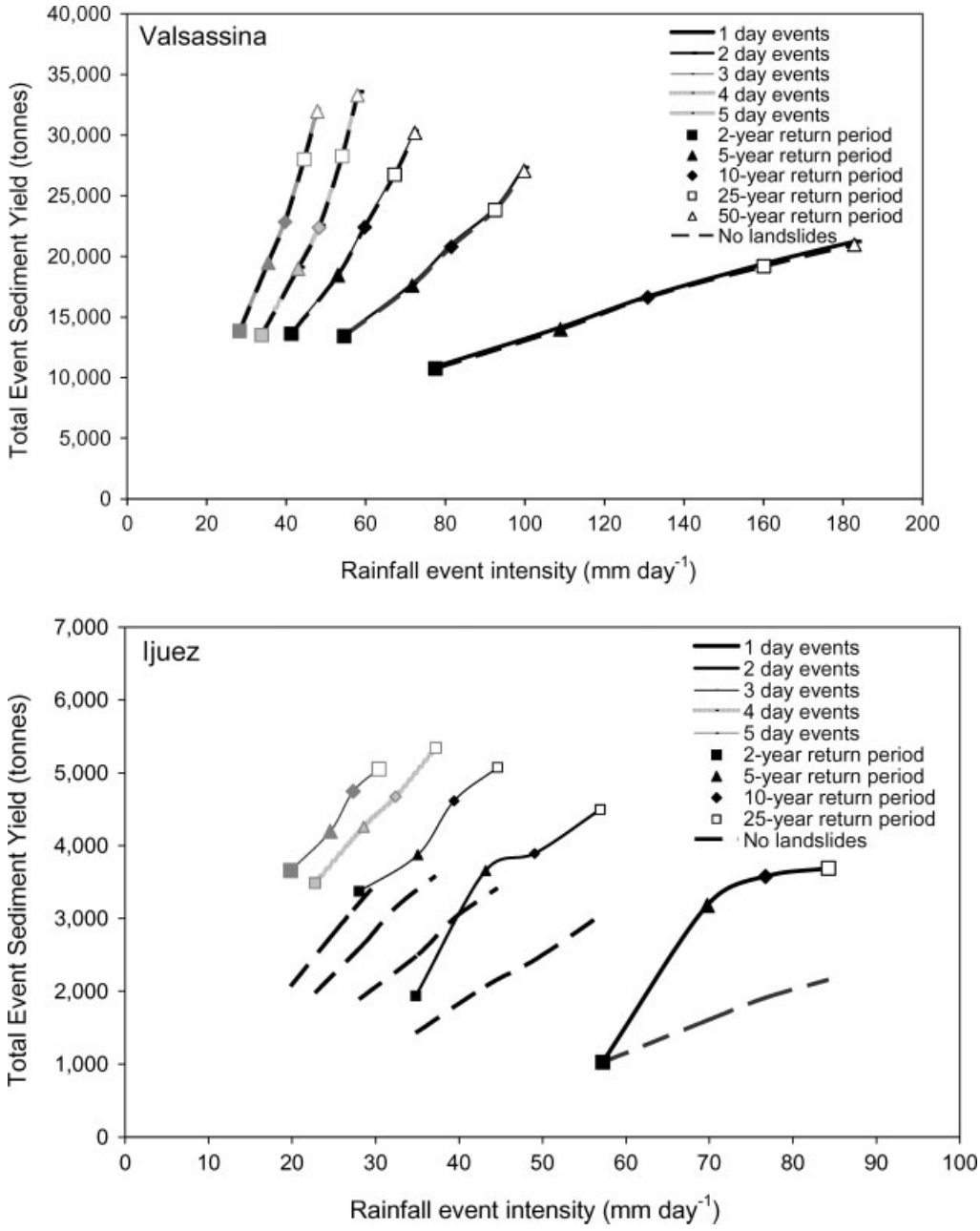

Figure 8. Relationship between total event sediment yield (with and without the landslide contribution) and rainfall event intensity for different event durations and return periods, for the central-peak rainfall pattern, for the Valsassina and Ijuez catchments

in 2005 (Dieter Rickenmann, personal communication) shows debris flow volume varying as a function of rainfall intensity for the 2·6-km^2 Wartschenbach catchment in Eastern Tyrol with a convex-upwards relationship. (In this case, the source of the sediment is not limited to shallow failures.) An event with a rainfall intensity of about 55 mm h^{-1} lasting approximately 30 min produced about 45 000 m^3 of debris flow material whilst an event of 6 mm h^{-1} lasting 6·5 h produced about 10 000 m^3 of material. Similarly, Figure 5 of Mao *et al*. (2006) shows event sediment yield as a function of return period for two mountain streams subject to debris flows and large bed load movements. In their published form, plotted on logarithmic axes, the relationships of Mao *et al*. have a convex-upwards nature but on linear axes they rather more resemble those curves of Figure 8 which have a linear form.

Landslide magnitude relationships

Figure 9 shows the number of landslides simulated as a function of rainfall event duration and intensity for the central-peak rainfall distribution for the Valsassina and Ijuez catchments. Log scales are used in conformance with practice in the literature but the results are also shown with linear scales as the wider spread of the data points allows easier visual interpretation. On this basis, it is possible to plot rainfall intensity–duration curves (grey lines in the diagram) which define different levels of landslide magnitude as quantified by the number of landslides. Also shown are the global threshold relationships

Copyright © 2011 John Wiley & Sons, Ltd.

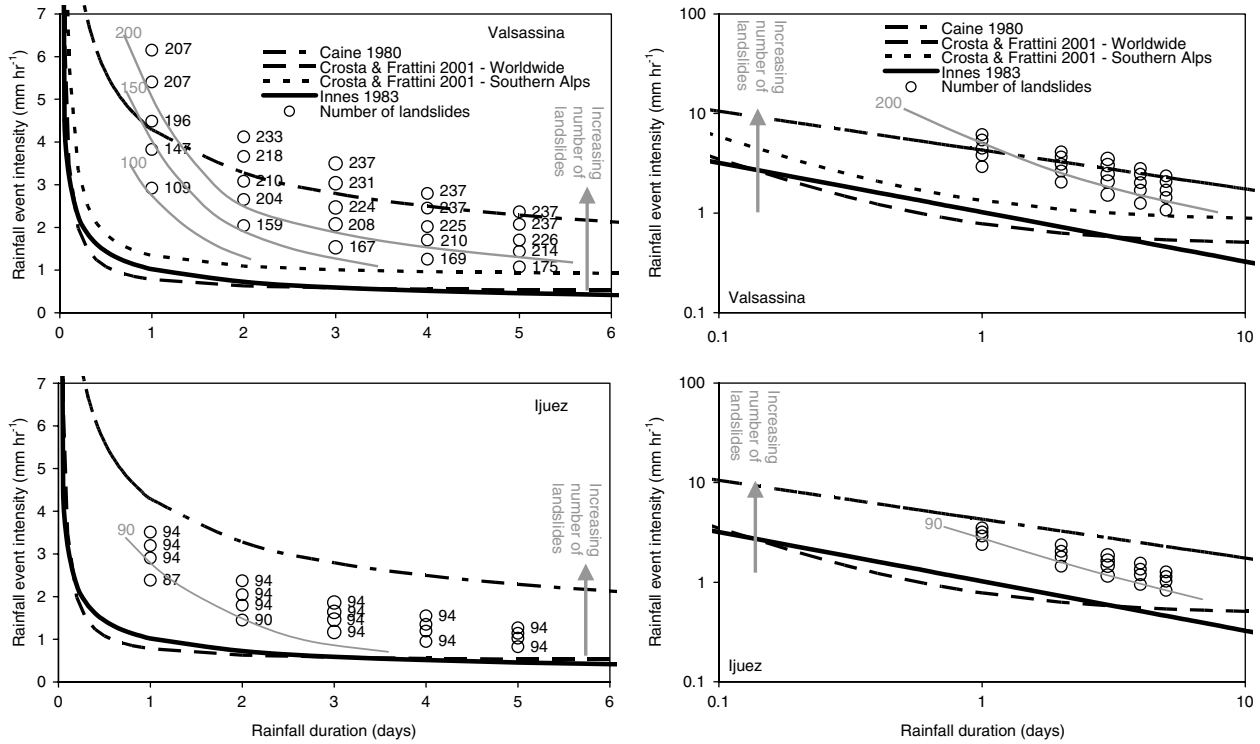

Figure 9. Relationship between the number of landslides and rainfall event intensity and duration for the central-peak rainfall pattern, in comparison with published threshold curves. Lines of equal numbers of landslides are fitted by eye. Results are shown for the Valsassina and Ijuez catchments, with linear and logarithmic scales

of Caine (1980) (Equation (1)), Innes (1983) and Crosta and Frattini (2001) (Equation (2)) and (on the Valsassina plots) the local threshold for the Southern Italian Alps of Crosta and Frattini (2001) (Equation (2)) (black lines in the diagram). Since, in this study, all the simulation rainfall events generated landslides, it was not possible to define a simulation threshold curve for landslide occurrence which could be compared directly with the literature curves. However, the landslide magnitude curves (grey lines) have the same general form as the literature curves, i.e. the intensity required to generate a given magnitude declines as duration increases. It should also be expected that the simulation points at least lie above the literature curves. This is the case for the global threshold curves of Innes (1983) and Crosta and Frattini (2001), and the Valsassina data are similarly in good correspondence with Crosta and Frattini's (2001) local threshold for the Southern Italian Alps. The Caine threshold on the other hand exceeds most of the simulation data but this is in agreement with Rossi *et al*. (2006) and Guzzetti *et al*. (2008) who also found the Caine threshold to be an overestimate. The reasons may lie in the data used by Caine, which were from a range of environments and antecedent moisture conditions, with precipitation from hourly, daily and monthly records. Intensities were calculated from averaging the durations and rainfall recorded for the events.

A feature of the logarithmic plots in Figure 9 is that the simulation data curves are steeper than the literature threshold curves. Thus, for long duration, low-intensity rainfall events, landslides could potentially be simulated at conditions below the literature threshold curves. This may be an artefact of the SHETRAN model as the trend is evident for both the Valsassina and the Ijuez catchments. However, Rossi *et al*. (2006) also found that, on a log–log intensity–duration plot, local thresholds were steeper than regional and global thresholds, a pattern which they attributed to differences in rainfall sampling resolution. In general, incompleteness of rainfall data (lack of short or long duration values) will cause the threshold curves to rotate preferentially in a clockwise or anticlockwise direction (Crosta and Frattini, 2001). Further, Rossi *et al*. (2006) found that, except for Caine's (1980) threshold, global thresholds were generally the lowest thresholds in the literature. Regional thresholds were higher than global thresholds and local thresholds were in turn higher than regional thresholds. The relative position of the curves can also be affected by the way in which rainfall intensity is calculated (Crosta and Frattini, 2001). Thus, downward shifting of the threshold curves can result from using total rainfall event intensity (the total event rainfall divided by the event duration, as in Figure 9), rather than maximum event intensity (determined for a limited time interval usually, but not necessarily, close to the time when landslides occurred) (Crosta and Frattini, 2001). Thresholds based on maximum intensity take no account of total event duration, antecedent rainfall or rainfall pattern and tend to underestimate the amount of rainfall needed to trigger landslides. Total event intensity, on the other hand, does not take short duration–high-intensity storms into account and thresholds based on total event intensity

Copyright © 2011 John Wiley & Sons, Ltd.

therefore tend to underestimate the rainfall intensity required to trigger landslides. It is important, therefore, when developing or applying threshold or magnitude relationships, to define their applicability (global, regional or local), the rainfall intensity (maximum or total event intensity) and the rainfall sampling resolution.

The landslide magnitude curves in Figure 9 advance our predictive capability beyond the existing threshold curves (which indicate only whether or not landslides should occur) and show how model simulations can be used to relate landslide magnitude to rainfall frequency. Not only numbers of landslides but location within a catchment, proportion of the catchment affected, likely timing of occurrence and impact in terms of sediment yield can be determined for given rainfall conditions. This type of information could be a helpful contribution to the wider process of landslide hazard assessment and forecasting.

CONCLUSIONS

Determining the extent of shallow landslide occurrence as a function of rainfall return period improves our ability to assess landslide hazard for specified conditions and raises the possibility of issuing warnings of landslide magnitude on the basis of weather forecasts. This study has investigated the use of a shallow landslide sediment yield model to quantify the magnitude of landslide events and their sediment yield as a function of rainfall return period, for rainfalls of different combinations of intensity and duration. The model transfers landslide material to the channel system via hillslope or unconfined debris flows but does not account for debris flows which may develop within the channel system. The principal conclusions are:

1. For a given event duration, simulated landslide magnitude becomes progressively less sensitive to return period as return period increases. Similarly, for an event of given return period, landslide magnitude becomes less sensitive to event duration as duration increases. These are not unrealistic patterns, although they may not be typical of all catchments. Nevertheless, it is likely that the patterns have been exaggerated by the model limitations and parameter evaluation.
2. As modelled, the temporal distribution of rainfall within an event (central peak, constant, early peak, late peak) has a significant effect on the simulated number of landslides and on the timing of their occurrence. Although the precise effects remain to be confirmed by field study, the result suggests that it is important to base the overall method on the characteristic rainfall pattern of events likely to trigger landslides in a region.
3. The contribution of shallow landsliding to catchment sediment yield can be quantified as a function of the rainfall characteristics. Downstream impacts of landslides can thus be determined for specified conditions as part of hazard assessment. For the two test sites, the contribution is likely to be small for the Valsassina catchment and moderate for the Ijuez catchment.
4. Rainfall intensity–duration curves can be determined which define different levels of landslide magnitude: as with threshold curves, the intensity required to generate a given magnitude declines as duration increases. The data are generally consistent with published threshold curves but it is important to define applicability (global, regional or local), rainfall intensity and rainfall sampling resolution.

The study has established and demonstrated a methodology by which a physically based, spatially distributed model can be used to relate landslide magnitude to rainfall frequency, thereby advancing our predictive capability beyond the threshold curves and providing information for use in landslide hazard assessment and forecasting. However, there remain a number of uncertainties in the procedure. These include uncertainty in quantifying rainfall of given return periods (especially large-return periods) from limited data records, uncertainty in generating the landslide response (as a function of model and parameter uncertainty) and uncertainty arising from processes and conditions not fully considered here, such as antecedent soil moisture content. Further applications and developments to reduce this uncertainty are needed to refine the approach. Given the significant control on landslide occurrence exercised by antecedent soil moisture content, a particularly useful development would be a set of simulations relating landslide magnitude to, for example, the duration of the rain-free period preceding a rainfall event. Similarly, considerably more field data on landslide occurrence and its relationship to rainfall return period are required so that simulations such as those reported here can be checked and calibrated.

ACKNOWLEDGEMENTS

The authors thank Professor Giovanni Crosta and Dr Paolo Frattini (University of Milan-Bicocca) for their advice and interest in the simulation results. The LESS-LOSS (Risk Mitigation for Earthquakes and Landslides) project was funded by the Framework Programme 6 Thematic Sub-priority "Global Change and Ecosystems" of the European Commission Research Directorate General, under Contract Number GOCE-CT-2003-505448, and this support is gratefully acknowledged. Professor Roy Sidle and an anonymous referee are thanked for their comments, which have greatly helped to improve the paper.

REFERENCES

Adams R, Parkin G, Rutherford JC, Ibbitt RP, Elliott AH. 2005. Using a rainfall simulator and a physically based hydrological model to investigate runoff processes in a hillslope. *Hydrological Processes* **19**: 2209–2223.

Acharya G, Cochrane TA, Davies T, Bowman E. 2009. The influence of shallow landslides on sediment supply: a flume-based investigation using sandy soil. *Engineering Geology* **109**: 161–169.

Copyright © 2011 John Wiley & Sons, Ltd.

Bathurst JC, Sheffield J, Vicente C, White SM, Romano N. 2002. Modelling large basin hydrology and sediment yield with sparse data: the Agri basin, southern Italy. In *Mediterranean Desertification: A Mosaic of Processes and Responses*, Geeson NA, Brandt CJ, Thornes JB (eds). Wiley: Chichester; 397–415.

Bathurst JC, Crosta G, García-Ruiz JM, Guzzetti F, Lenzi M, Ríos S. 2003. DAMOCLES: debrisfall assessment in mountain catchments for local end-users. In *Proceedings of the 3rd International Conference on Debris-Flow Hazards Mitigation: Mechanics, Prediction and Assessment*, vol. 2, Rickenmann D, Chen C-L (eds). Millpress: Rotterdam; 1073–1083.

Bathurst JC, Ewen J, Parkin G, O'Connell PE, Cooper JD. 2004. Validation of catchment models for predicting land-use and climate change impacts. 3. Blind validation for internal and outlet responses. *Journal of Hydrology* **287**: 74–94.

Bathurst JC, Moretti G, El-Hames A, Moaven-Hashemi A, Burton A. 2005. Scenario modelling of basin-scale, shallow landslide sediment yield, Valsassina, Italian Southern Alps. *Natural Hazards and Earth System Sciences* **5**: 189–202.

Bathurst JC, Burton A, Clarke BG, Gallart F. 2006. Application of the SHETRAN basin-scale, landslide sediment yield model to the Llobregat basin, Spanish Pyrenees. *Hydrological Processes* **20**: 3119–3138.

Bathurst JC, Moretti G, El-Hames A, Beguería S, García-Ruiz JM. 2007. Modelling the impact of forest loss on shallow landslide sediment yield, Ijuez river catchment, Spanish Pyrenees. *Hydrology and Earth System Sciences* **11**: 569–583.

Beguería S. 2006. Changes in land cover and shallow landslide activity: a case study in the Spanish Pyrenees. *Geomorphology* **74**: 196–206.

Beven KJ. 2001. *Rainfall-runoff modelling: the primer*. Wiley: Chichester; 360 pp.

Beven K, Binley A. 1992. The future of distributed models: model calibration and uncertainty prediction. *Hydrological Processes* **6**: 279–298.

Brunetti MT, Peruccacci S, Rossi M, Luciani S, Valigi D, Guzzetti F. 2010. Rainfall thresholds for the possible occurrence of landslides in Italy. *Natural Hazards and Earth System Sciences* **10**: 447–458.

Burton A, Bathurst JC. 1998. Physically based modelling of shallow landslide sediment yield at a catchment scale. *Environmental Geology* **35**: 89–99.

Caine N. 1980. The rainfall intensity-duration control of shallow landslides and debris flows. *Geografiska Annaler* **62A**: 23–27.

Chen Chien-Yuan, Chen Tien-Chien, Yu Fan-Chieh, Yu Wen-Hui, Tseng Chun-Chieh. 2005. Rainfall duration and debris-flow initiated studies for real-time monitoring. *Environmental Geology* **47**: 715–724.

Crosta GB, Frattini P. 2001. Rainfall thresholds for triggering soil slips and debris flow. In *Proceedings of the 2nd EGS Plinius Conference on Mediterranean Storms, 16–18th October 2000, Sienna, Italy*. Mugnai A, Guzzetti F, Roth G. (eds) 463–487. GNDCI pub. n 2547, Perugia', 529 p.

Crozier MJ, Eyles RJ. 1980. Assessing the probability of rapid mass movement. In *Proceedings of the 3rd Australia-New Zealand Conference on Geomechanics*. New Zealand Institution of Engineers Proceedings of Technical Groups **6**, Issue 1(G), Part 2: 2·47–2·51.

Crozier MJ, Glade T. 1999. Frequency and magnitude of landsliding: fundamental research issues. *Zeitschrift für Geomorphologie, Supplement-Band* **115**: 141–155.

D'Agostino V, Marchi L. 2001. Debris flow magnitude in the Eastern Italian Alps: data collection and analysis. *Physics and Chemistry of the Earth (C)* **9**: 657–663.

Dhakal AS, Sidle RC. 2004. Distributed simulations of landslides for different rainfall conditions. *Hydrological Processes* **18**: 757–776.

Ewen J, Parkin G. 1996. Validation of catchment models for predicting land-use and climate change impacts. 1. Method. *Journal of Hydrology* **175**: 583–594.

Ewen J, Parkin G, O'Connell PE. 2000. SHETRAN: distributed river basin flow and transport modeling system. Proceedings of the American Society of Civil Engineers. *Journal of Hydrologic Engineering* **5**: 250–258.

Falorni G, Leoni L, Benedetti A, Catani F, Rudari R, Pellegrino D, Ciminelli M, Giannoni F. 2007. PREVIEW Service 2: forecasting shallow rapid landslides. *Geophysical Research Abstracts* **9**: EGU2007–A-09431. (Abstract only).

Frattini P, Crosta G, Sosio R. 2009. Approaches for defining thresholds and return periods for rainfall-triggered shallow landslides. *Hydrological Processes* **23**: 1444–1460.

García-Ruiz JM, Arnáez J, White SM, Lorente A, Beguería S. 2000. Uncertainty assessment in the prediction of extreme rainfall events: an example from the central Spanish Pyrenees. *Hydrological Processes* **14**: 887–898.

Gorsevski PV, Gessler PE, Boll J, Elliott WJ, Foltz RB. 2006. Spatially and temporally distributed modelling of landslide susceptibility. *Geomorphology* **80**: 178–198.

Guimarães RF, Montgomery DR, Greenberg HM, Fernandes NF, Gomes RAT, de Carvalho Júnior OA. 2003. Parameterization of soil properties for a model of topographic controls on shallow landsliding: application to Rio de Janeiro. *Engineering Geology* **69**: 99–108.

Guzzetti F, Peruccacci S, Rossi M, Stark CP. 2008. The rainfall intensity–duration control of shallow landslides and debris flows: an update. *Landslides* **5**: 3–17.

Hicks DM, Gomez B, Trustrum NA. 2000. Erosion thresholds and suspended sediment yields, Waipaoa River Basin, New Zealand. *Water Resources Research* **36**: 1129–1142.

Iida T. 2004. Theoretical research on the relationship between return period of rainfall and shallow landslides. *Hydrological Processes* **18**: 739–756.

Imaizumi F, Sidle RC. 2007. Linkage of sediment supply and transport processes in Miyagawa dam catchment, Japan. *Journal of Geophysical Research* **112**: F03012, DOI:10.1029/2006JF000495.

Innes JL. 1983. Debris flows. *Progress in Physical Geography* **7**: 469–501.

Jakob M, Bovis M, Oden M. 2005. The significance of channel recharge rates for estimating debris-flow magnitude and frequency. *Earth Surface Processes and Landforms* **30**: 755–766.

Johnson AC, Swanston DN, McGee KE. 2000. Landslide initiation, runout, and deposition within clearcuts and old-growth forests of Alaska. *Journal of the American Water Resources Association* **36**: 17–30.

Lorente A, Beguería S, Bathurst JC, García-Ruiz JM. 2003. Debris flow characteristics and relationships in the Central Spanish Pyrenees. *Natural Hazards and Earth System Sciences* **3**: 683–692.

Luino F. 2005. Sequence of instability processes triggered by heavy rainfall in the northern Italy. *Geomorphology* **66**: 13–39.

Lukey BT, Sheffield J, Bathurst JC, Hiley RA, Mathys N. 2000. Test of the SHETRAN technology for modelling the impact of reforestation on badlands runoff and sediment yield at Draix, France. *Journal of Hydrology* **235**: 44–62.

Mao L, Cavalli M, Comiti F, Marchi L, Arattano M. 2006. Long-term monitoring of bedload and debris flows in two small catchments of the Eastern Italian Alps. In *Monitoring, Simulation, Prevention and Remediation of Dense and Debris Flows*, Lorenzini G, Brebbia CA, Emmanouloudis DE (eds). WIT Press: Southampton; 147–157.

Montgomery DR, Dietrich WE. 1994. A physically based model for the topographic control on shallow landsliding. *Water Resources Research* **30**: 1153–1171.

Page M, Trustrum N, Brackley H, Baisden T. 2004. Erosion-related soil carbon fluxes in a pastoral steepland catchment, New Zealand. *Agriculture, Ecosystems and Environment* **103**: 561–579.

Preston NJ, Crozier MJ. 1999. Resistance to shallow landslide failure through root-derived cohesion in east coast hill country soils, North Island, New Zealand. *Earth Surface Processes and Landforms* **24**: 665–675.

Reichenbach P, Cardinali M, De Vita P, Guzzetti F. 1998. Regional hydrological thresholds for landslides and floods in the Tiber River Basin (central Italy). *Environmental Geology* **35**: 146–159.

Reid LM, Page MJ. 2002. Magnitude and frequency of landsliding in a large New Zealand catchment. *Geomorphology* **49**: 71–88.

Rossi M, Peruccacci S, Guzzetti F. 2006. A review of rainfall thresholds for the initiation of landslides. *Geophysical Research Abstracts* **8**: EGU06–A-02323. (Abstract only).

Schmidt J, Turek G, Clark MP, Uddstrom M, Dymond JR. 2008. Probabilistic forecasting of shallow, rainfall-triggered landslides using real-time numerical weather predictions. *Natural Hazards and Earth System Sciences* **8**: 349–357.

Sidle RC, Pearce AJ, O'Loughlin CL. 1985. *Hillslope stability and land use*. *Water Resources Monograph Series 11*, American Geophysical Union: Washington DC.

Sidle RC, Ochiai H. 2006. *Landslides: Processes, Prediction, and Land Use*. *Water Resources Monograph 18*, American Geophysical Union: Washington DC.

Wilkinson PL, Anderson MG, Lloyd DM. 2002. An integrated hydrological model for slope stability. *Earth Surface Processes and Landforms* **27**: 1267–1283.

Wu W, Sidle RC. 1995. A distributed slope stability model for steep forested basins. *Water Resources Research* **31**: 2097–2110.

Copyright © 2011 John Wiley & Sons, Ltd.